Chinese Journal of Chemical Engineering 42 (2022) 120–129

Contents lists available at ScienceDirect

Chinese Journal of Chemical Engineering

journal homepage: www.elsevier.com/locate/CJChE

Full Length Article

Nitrogen rejection from low quality natural gas by pressure swing adsorption experiments and simulation using dynamic adsorption isotherms

Xinran Zhang [1], Hua Shang [1], Jiangfeng Yang [1,2,*], Libo Li [1,2], Jinping Li [1,2]

[1] *Research Institute of Special Chemicals, College of Chemistry and Chemical Engineering, Taiyuan University of Technology, Taiyuan 030024, China*
[2] *Shanxi Key Laboratory of Gas Energy Efficient and Clean Utilization, Taiyuan 030024, China*

ARTICLE INFO

Article history:
Received 1 May 2021
Received in revised form 23 June 2021
Accepted 25 June 2021
Available online 9 September 2021

Keywords:
Natural gas
Silicalite-1
Simulation
Dynamic adsorption
Pressure swing adsorption process

ABSTRACT

In order to remove N_2 from low quality natural gas, a mathematical model has been established by Aspen adsorption, using the CH_4-selective sorbent silicalite-1 pellets. The dynamic adsorption isotherm was first simulated by breakthrough simulation of a CH_4/N_2 mixture at different adsorption pressures and feed flow rates based on breakthrough experiments. The resulting simulated CH_4 dynamic adsorption amounts were very close to the experimental data at three different adsorption pressures (100, 200, and 300 kPa). Moreover, a single-bed, three-step pressure swing adsorption (PSA) experiment was performed, and the results were in good agreement with the simulated data, further corroborating the accuracy of the gas dynamic adsorption isotherm obtained by the simulation method. Finally, based on the simulated dynamic adsorption isotherm of CH_4 and N_2, a four-bed, eight-step PSA process has been designed, which enriched 75% (vol) CH_4 and 80% (vol) CH_4 to 95% (vol) and 99% (vol), and provided 99% (vol) recovery.

1. Introduction

Natural gas is one of the important fossil fuels, and it is cleaner than coal or oil, having the highest H/C ratio, and its burning produces the least CO_2 per unit of energy, moreover, its lower sulfur and nitrogen contents also lead to lower SO_x and NO_x emissions [1–3]. Faced with increasing energy demand in today's global market and increasingly severe environmental problems, the effective use of natural gas is even more critical [4,5]. However, natural gas is a mixture of multiple gases, its main component is CH_4, which usually accounts for 75%–90% (vol) of the total, but N_2 is a common inert component, sometimes even reaching 25% (vol), greatly reducing the calorific value and increasing the transportation cost of natural gas, and so needs to be pre-separated [6–11]. The separation of N_2 and CH_4 presents a significant challenge due to their relatively similar physical properties; they are both nonpolar gases with similar kinetic diameters (0.38 nm for CH_4 and 0.364 nm for N_2) [12–14].

Normally, cryogenic distillation is a useful method for rejecting nitrogen, and is widely used commercially, but due to its high energy consumption, it is only suitable for large-scale processing [15,16]. In contrast, pressure swing adsorption (PSA) is an alternative technology with promising potential because of its low energy consumption, relatively simple operation, and low equipment investment [17–19]. However, it should be noted that currently used adsorbents rarely achieve the desired separation effect, and need to be assisted by an efficient PSA separation process. Research on PSA usually requires a combination of experiments and mathematical modeling in order to design and optimize the process or to evaluate the effect of the adsorbent, because the mathematical model can provide a good window for observing and understanding dynamic adsorption and desorption, effectively reducing the experimental cost, shortening the process cycle, and serving to guide practice by theory [20].

For example, the model can be used to estimate product recovery and purity, to explore the thermodynamics and kinetics of the adsorbent, to observe the material and temperature distribution in the bed, to study the influence of process parameters (feed rate, adsorption pressure, *etc.*) on PSA, and so on [21–28]. Thus, it is essential to establish an accurate mathematical model. Xiao *et al.* [18] enriched the CH_4 in a mixed gas of 75% (vol) CH_4/25% (vol)

* Corresponding author at: Research Institute of Special Chemicals, College of Chemistry and Chemical Engineering, Taiyuan University of Technology, Taiyuan 030024, China.
E-mail address: yangjiangfeng@tyut.edu.cn (J. Yang).

https://doi.org/10.1016/j.cjche.2021.06.028
1004-9541/

N_2 to 90% (vol) purity, and achieved 90% (vol) recovery, using a kinetically nitrogen-selective molecular sieve carbon, MSC-3K 172, in a dual-reflux (DR) PSA process. Erden and co-workers [29] compared the results of three different four-bed, four-step PSA cycles, namely the heavy-end HR (HEHR), HEHR plus recycle (HEHR-Rec), and light-end HR plus Rec (LEHR–Rec), and by adopting the HEHR-Rec PSA cycle and BPL activated carbon, they succeeded in enriching the CH_4 in a mixed gas of 88% (vol) CH_4/12% (vol) N_2 to 99.4% (vol) purity with a recovery of 99.2% (vol).

According to our investigation, there is no PSA study on CH_4-selective molecular sieve to enrich CH_4 from a high ratio of CH_4/N_2 mixture so far, and from our previous research [30], as a CH_4-selective sorbent, silicalite-1 pellets exhibit very good CH_4/N_2 separation performance. Moreover, the shape of these pellets avoids a huge pressure drop in the adsorption column. Indeed, we have proven that silicalite-1 pellets have good application prospects in the enrichment of CH_4 in low concentration coalbed gas, and a two-bed, six-step PSA process was designed to enrich 20% (vol) and 30% (vol) CH_4 to 40% (vol) and 57% (vol) with recoveries above 80% (vol) through the experiment and simulation method. In this work, through comparing breakthrough experiments and simulations, a 75% (vol) CH_4/25% (vol) N_2 gas dynamic adsorption isotherm of silicalite-1 pellets has been obtained and verified, considering the competitive adsorption of CH_4 and N_2 in the adsorption bed. Based on the dynamic adsorption isotherm, a four-bed, eight-step PSA has been designed to reject N_2 from low-quality natural gas.

2. Experimental

2.1. Examination of the adsorption performances of the pure gas components

CH_4 and N_2 pure component adsorption isotherm data on silicalite-1 were acquired in our previous work [31]. They could be fitted by the Langmuir-Freundlich (Eq. (1)) isotherm model in the framework of Aspen adsorption.

$$q_i = \frac{a_{1i} P_i^{a_{2i}} e^{a_{3i}/T}}{1 + a_{4i} P_i^{a_{2i}} e^{a_{3i}/T}} \quad (1)$$

Here, q_i is the amount of component i adsorbed, P_i is the partial pressure of component i, and a_1, a_2, a_3, and a_4 are constants.

2.2. Breakthrough experiments

The experimental set-up for mixed-gas dynamic breakthrough is shown in Fig. 1. The inlet gas was 75% (vol) CH_4/25% (vol) N_2 and 99.999% (vol) He, and each adsorption column (35 cm × 2.2 cm) was filled with adsorbent pellets (98 g). The physical properties of the adsorption bed, adsorbent, and gas are listed in Table 1 and Table 2, respectively. A gas mass spectrometer (Hiden Analytical, HPR-20 R&D) was used to monitor the composition of the outlet gas in real time, and a PC controlled the pneumatic valve and flow meter to realize automated control of the experiment. The adsorbent was activated at 423 K for 4 h, and then helium was used to purge the bed and lower the temperature until N_2 was not detected at the outlet; the temperature had then decreased to ambient (298 K).

2.3. The single-bed, three-step PSA experiment

In the PSA experiment, a Programmable Logic Controller controlled switching of the pneumatic valve to realize automated circulation of the PSA. A buffer tank was added at the outlets of the upper and lower ends of the adsorption column, and a CH_4 concentration tester was used to detect the average CH_4 concentration of the outlet gas. The PSA experiment comprised three steps: pressurization (PR), adsorption (AD), and vacuum (VU). Of these, PR and AD lasted for 130 s in total, VU lasted for 130 s, and the two adsorption beds alternately performed 40 cycles until the average CH_4 gas concentration was almost constant at the top and bottom of the adsorption bed.

3. Modeling

3.1. Binary component adsorption model

The binary component adsorption isotherm was predicted on the basis of the pure component adsorption isotherm, using ideal adsorbed solution theory (IAST) (Eqs. (2)–(6)), which is an effective

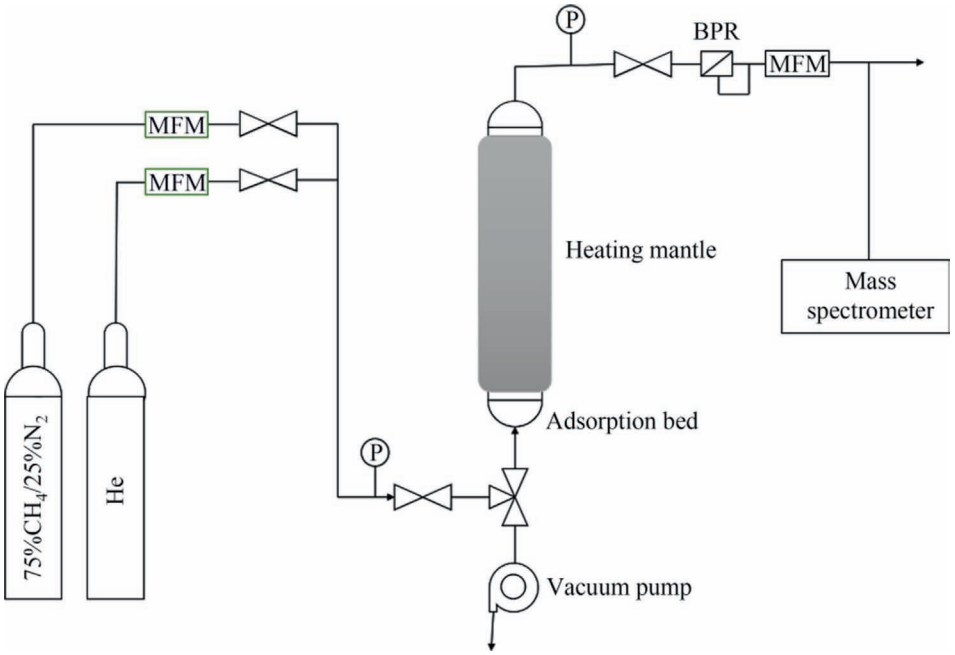

Fig. 1. The experimental device for dynamic breakthrough of mixed gas.

Table 1
Physical characteristics of adsorption bed and adsorbent

Parameters	Value
Bed height, H_0/m	0.35
Bed diameter, d/m	0.022
Bulk density, ρ_s/kg·m^{-3}	737
Bed void ratio, ε_b	0.46
Particle porosity, ε_p	0.3
Particle radius, r_p/m	7×10^{-4}
Average pore size, r_{pore}/m	2.7×10^{-9}

Table 2
Gas model parameters

Parameters	CH_4	N_2
adsorption heat, ΔH/kJ·mol^{-1}	−13	−15
dynamic viscosity, μ/N·s·m^{-2}	1.1×10^{-5}	1.8×10^{-5}
Molecular diffusion volume, D_V/cm^3·mol^{-1}	24.5	18.5

method based on a reasonable thermodynamic framework [13,32–37].

$$p_i = py_i = p_i^0 x \tag{2}$$

$$\sum_{i=1}^{n} x_i = 1, \sum_{i=1}^{n} y_i = 1 \tag{3}$$

$$q_i = q_T x_i \tag{4}$$

$$\frac{1}{q_T} = \sum_{i-1}^{n} \frac{x_i}{q_i^0} \tag{5}$$

$$\frac{\pi A}{RT} = \int_0^{p_i^0} \frac{q_i(p_i)}{p_i} \mathrm{d}p_i = \text{constant} \tag{6}$$

Here, p_i^0 is the standard-state pressure of pure component i corresponding to the spreading pressure of the mixture, q_T is the total amount adsorbed, and A is the specific surface area of the adsorbent.

Table 3
The effect of different values of Peclet number

Peclet	The type of gas flow
0	Fully mixed flow
<30	Obvious axial diffusion
>100	The gas flow is close to the plug flow, and the axial diffusion can be ignored
∞	Plug flow

3.2. Material, momentum, and energy balance models

Using Aspen adsorption to simulate breakthrough and PSA experiments, the adsorption bed, feed gas, product gas, valve, and gas pipe are shown in Fig. 2.

Material, momentum, and energy-balance models were established in the adsorption bed system, solved by the Upwind Difference. Because PSA is a relatively complex system, the following reasonable assumptions were made when establishing the mathematical model.

(1) All the gases were regarded as ideal.
(2) Only the temperature, pressure, and velocity gradient in the axial direction of the bed were considered, ignoring radial changes.
(3) Uniform bed void ratio and adsorbent particle porosity were included.

Material balance (Eq. (7)) included axial gas diffusion, convection, accumulation in the bed porosity, and mass transfer with the adsorbent [38].

$$-\varepsilon_b D_{ax} \frac{\partial^2 c_i}{\partial z^2} + \frac{\partial (v_g c_i)}{\partial z} + \left[\varepsilon_b + (1-\varepsilon_b)\varepsilon_p\right] \frac{\partial c_i}{\partial t} + \rho_s (1-\varepsilon_b) \frac{\partial q_i}{\partial t} = 0 \tag{7}$$

Here, ε_b is the bed void ratio, D_{ax} is the axial dispersion coefficient, c_i is the gas-phase concentration of component i, z is the axial distance of the adsorbent bed, v_g is the gas velocity, ε_p is the adsorbent particle porosity, t is the adsorption time, and q_i is the adsorbed concentration of component i.

As shown in Table 3, the degree of axial gas diffusion was determined by the type of gas flow, which was evaluated by the Peclet number (Eqs. (8)–(10)) [27].

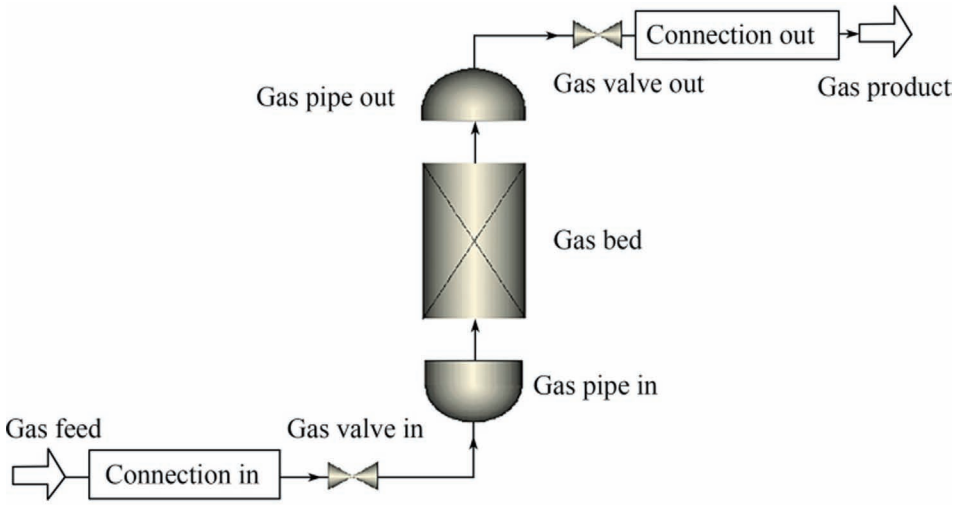

Fig. 2. Aspen Adsorption internal configuration diagram of breakthrough simulation.

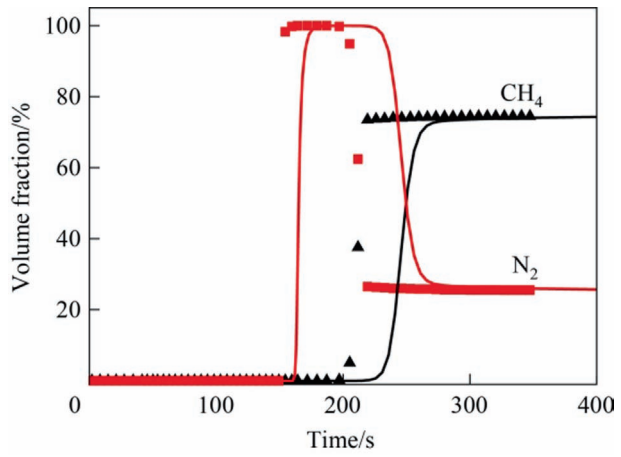

Fig. 3. 75% (vol) CH_4/25% (vol) N_2 breakthrough experiment (dotted line) and simulation (solid line) at 298 K, 100 kPa, 500 ml·min^{-1} feed rate, based on the static adsorption isotherm.

$$Pe = \frac{v_g H_0}{D_{ax}} \tag{8}$$

$$D_{ax} = 0.73D_m + \frac{v_g r_p}{\varepsilon_b\left(1 + 9.49\frac{\varepsilon_b D_m}{2v_g r_p}\right)} \tag{9}$$

$$D_m = \frac{0.1013T^{1.75}\sqrt{\frac{1}{M_A}+\frac{1}{M_B}}}{p\left(D_{V,A}^{1/3} + D_{V,B}^{1/3}\right)^2} \tag{10}$$

Here, D_m is the molecular diffusivity, M_A and M_B are the relative molecular masses of A and B, and $D_{V,A}$ and $D_{V,B}$ are the molecular diffusion volumes. In the following, the Peclet number was greater than 100, so the gas flow within the bed was regarded as a plug flow, and axial diffusion was ignored.

Gas energy balance (Eq. (11)) included energy convection, accumulation of heat, heat transfer from gas to solid, and heat transfer from gas to the wall [39].

$$c_{v,g}v_g\rho_g\frac{\partial T_g}{\partial t} + \varepsilon_b c_{v,g}\rho_g\frac{\partial T_g}{\partial t} + p\frac{\partial v_g}{\partial z} + h_f(T_g - T_s) + \frac{4h_w}{D_b}(T_g - T_0) = 0 \tag{11}$$

Here, T_g is the gas-phase temperature, T_0 is the ambient temperature, T_s is the solid-phase temperature, $c_{v,g}$ is the gas molar constant-volume heat capacity, ρ_g is the molar gas-phase density, h_f is the heat-transfer coefficient between the gas and solid, h_w is the heat-transfer coefficient between the gas and the wall, and D_b is the bed diameter.

Solid energy balance (Eq. (12)) included the accumulation of heat, the heat of adsorption, and gas–solid heat transfer from the gas to the solid [39].

$$c_{ps}\rho_s\frac{\partial T_s}{\partial t} + \rho_s\sum_{i=1}^{n}\left(\Delta H_i\frac{\partial q_i}{\partial t}\right) - h_f(T_g - T_s) = 0 \tag{12}$$

Here, c_{ps} is the specific heat capacity of the adsorbent, and ΔH_i is the heat of adsorption of component *i*.

The pressure drop in the bed was calculated according to the Ergun equation (Eq. (13)) [30].

$$\frac{\partial P}{\partial z} = -\left(\frac{1.5\times10^{-3}(1-\varepsilon_b)^2}{(2r_p\tau)^2\varepsilon_b^3}\mu v_g + 1.75\times10^{-5}\frac{M\rho_g(1-\varepsilon_b)}{2r_p\tau\varepsilon_b^3}v_g^2\right) \tag{13}$$

Here, τ is the adsorbent tortuosity factor, M is the molar mass, and μ is the dynamic gas viscosity.

3.3. Mass-transfer model

In the mass-transfer equation (Eq. (14)), it was assumed that the mass-transfer coefficient was constant, consisting of two parts: one was the mass-transfer resistance formed by the gas passing through the boundary layer between the gas phase and the solid phase, and the other was the diffusion resistance of the gas in the internal pores of the adsorbent particles [40].

$$\frac{\partial q_i}{\partial t} = k_i(q_{mi} - q_i); \quad \frac{1}{k_i} = \frac{r_p}{3k_{fi}} + \frac{r_p^2}{15D_{pi}} \tag{14}$$

Here, q_{mi} is the equilibrium adsorption amount, k_i is the mass-transfer coefficient, k_{fi} is the film-resistance coefficient, calculated according to Eq. (15), and D_{pi} is the effective gas-phase pore diffusion coefficient, calculated according to Eq. (16).

$$k_{fi} = Sh_i\frac{D_{mi}}{2r_p}; \quad Sh_i = 2 + 1.1Sc_i^{1/3}Re^{0.6}; \quad Sc_i = \frac{\mu}{D_{mi}\rho_g M} \tag{15}$$

Here, Sh_i is the Sherwood number, Sc_i is the Schmidt number, and Re is the Reynolds number.

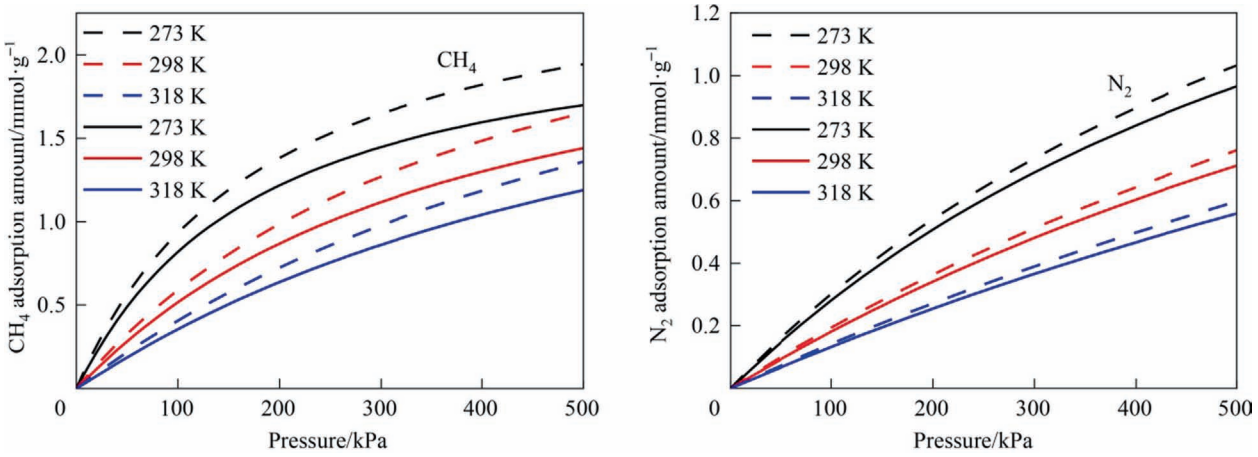

Fig. 4. Langmuir-Freundlich fitting curves of pure component static adsorption isotherms (dashed line) and adjusted adsorption isotherms (solid line) of CH_4 and N_2 at different temperatures.

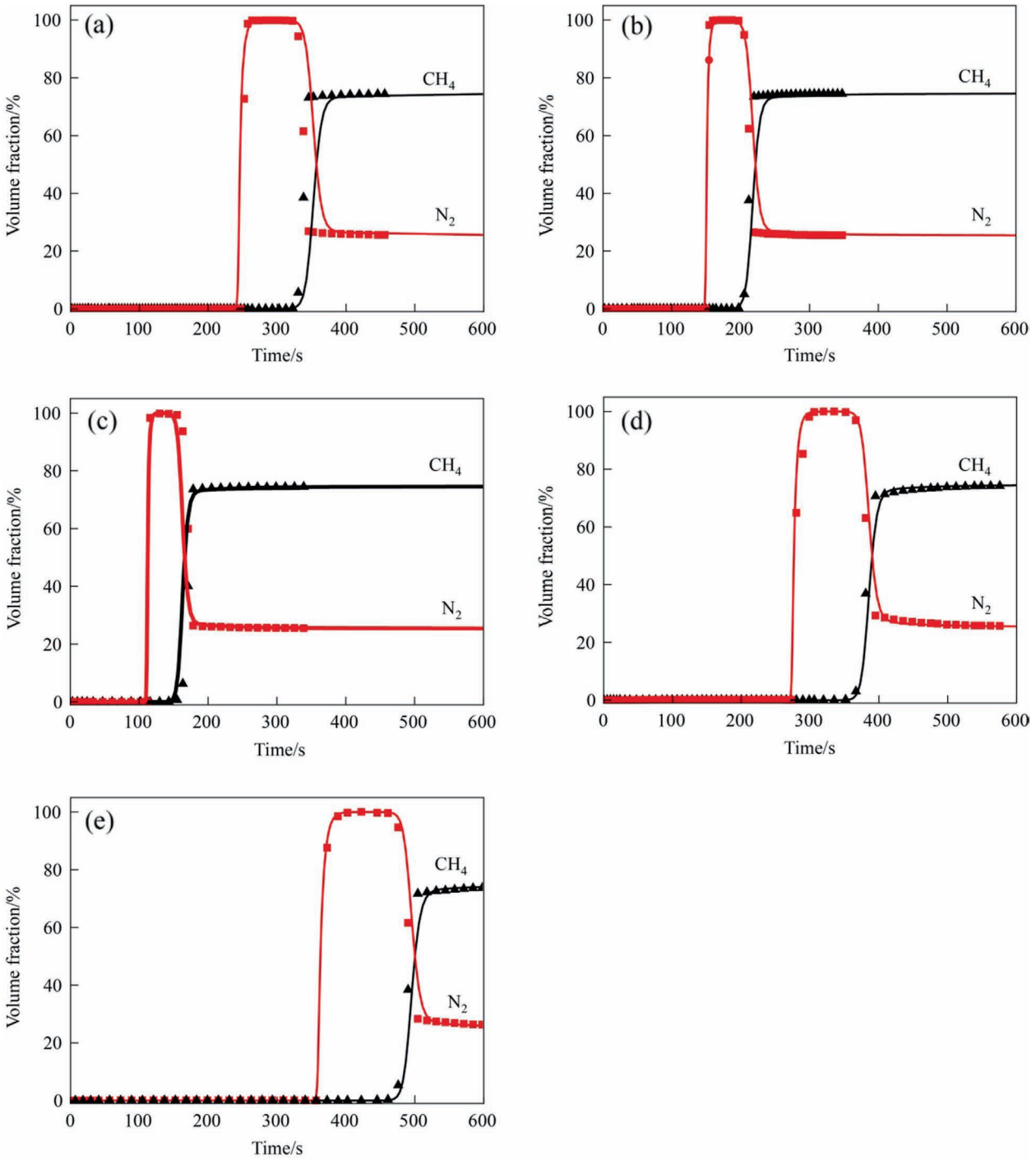

Fig. 5. 75% (vol) CH_4/25% (vol) N_2 breakthrough experiment (dotted line) and simulation (solid line) at 298 K (a) 100 kPa, 300 ml·min^{-1} (b) 100 kPa, 500 ml·min^{-1} (c) 100 kPa, 700 ml·min^{-1} (d) 200 kPa, 500 ml·min^{-1} (e) 300 kPa, 500 ml·min^{-1}, based on the adjusted adsorption isotherm (dynamic adsorption isotherm).

$$\frac{1}{D_{pi}}=\frac{\tau}{\varepsilon_p}\left(\frac{1}{D_{Ki}}+\frac{1}{D_{mi}}\right);\quad D_{Ki}=97r_p\left(\frac{T}{M_i}\right)^{0.5} \tag{16}$$

Here, D_{ki} is the Knudsen diffusion coefficient, and D_{mi} is the multi-component molecular diffusion coefficient.

4. Results and Discussion

4.1. Breakthrough experiment and simulation

First, the breakthrough experiment was simulated at 100 kPa, 298 K, and 500 ml·min^{-1} feed (Fig. 3), based on Langmuir-Freundlich fitting curves of pure component static adsorption isotherms (Fig. 4, dashed line). The breakthrough times of N_2 and CH_4 were thereby evaluated as 150 s and 200 s, respectively. In the simulation, the breakthrough times of N_2 and CH_4 were both longer than those in the experiment, at 162 s and 228 s, respectively, because the dynamic adsorption capacity of the adsorbent was indeed smaller than its static adsorption capacity. Moreover, the inhomogeneity of the radial adsorption amount inside the adsorption column could be regarded as negligible during the experiment, due to the small diameter of the column and the high adsorption rate of the adsorbent. Hence, the decrease in adsorption capacity was only due to the dynamic adsorption process. This result

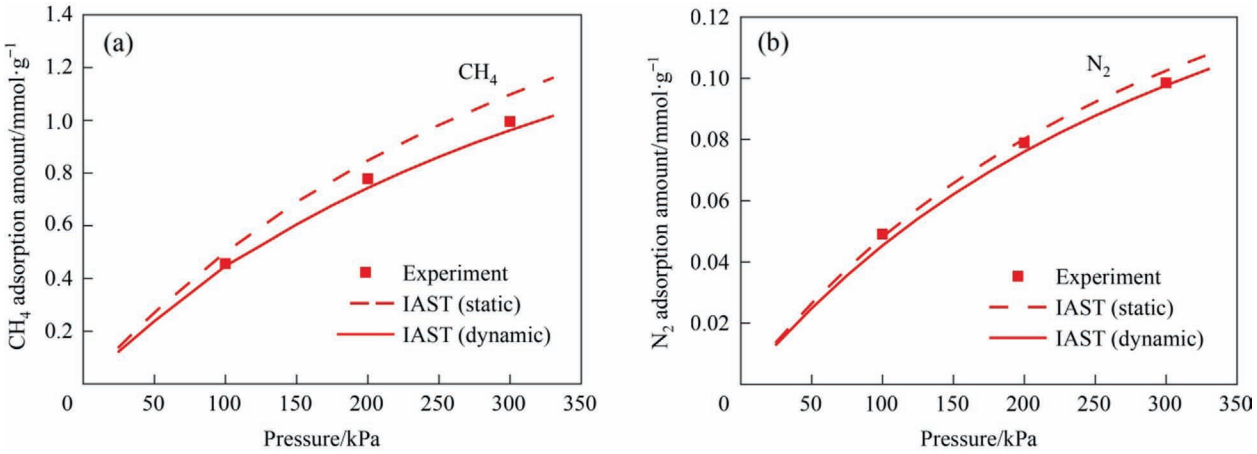

Fig. 6. CH_4 (a) and N_2 (b) dynamic adsorption isotherm of 75% (vol) CH_4/25% (vol) N_2 gas at 298 K on silicalite-1 pellets.

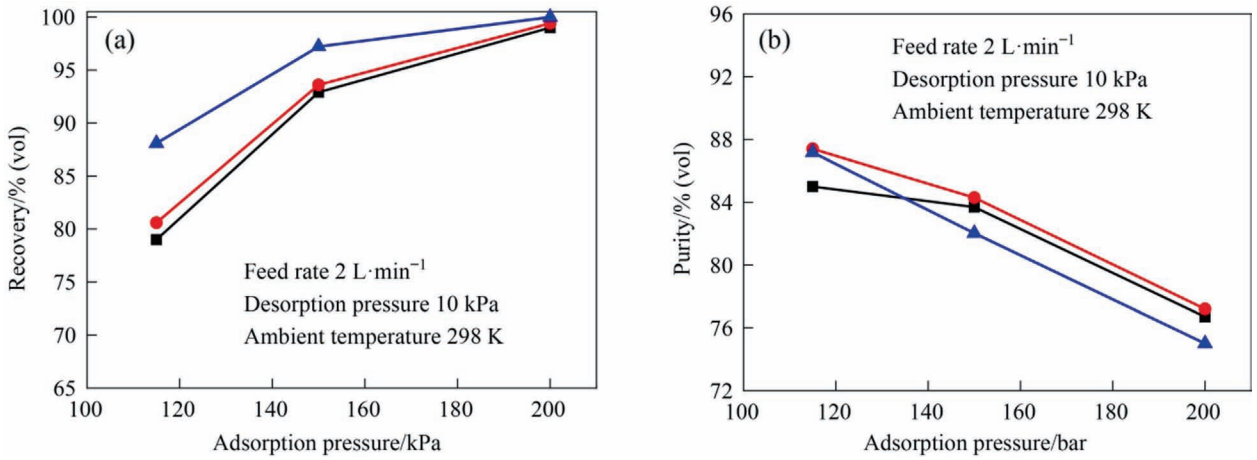

Fig. 7. Comparison of PSA experiment (black) and simulation (red and blue) results, red and blue line respectively represent the simulation using dynamic and static adsorption isotherm. CH_4 recovery (a) and CH_4 purity (b).

Table 4
Comparison of step time between PSA experiment and simulation

P/kPa	Feed rate/L·min^{-1}	Experiment *T*/s			Simulation (dynamic) *T*/s			Simulation (static) *T*/s		
		PR	AD	VU	PR	AD	VU	PR	AD	VU
115	1.50	100	30	130	100	30	130	109	21	130
115	1.75	87	43	130	86	44	130	93	37	130
115	2.00	75	55	130	75	55	130	81	49	130
150	2.00	95	35	130	95	35	130	103	27	130
200	2.00	120	10	130	120	10	130	130	0	130

Note: *P* is adsorption pressure, and *T* is time.

showed that the simulation may incur great errors if the static adsorption isotherm was used for the dynamic adsorption process.

We attempted to simulate the dynamic adsorption isotherm from the relatively simple dynamic adsorption process of gas breakthrough. IP_1 is known to be the factor showing the least correlation with adsorption pressure and temperature in the Langmuir-Freundlich isotherm model. Therefore, IP_1 was adjusted to decrease the gas adsorption capacity of the adsorbent (Fig. 4, solid line), and simulated breakthrough curves consistent with the experiment at different adsorption pressures and feed flow rates were thereby obtained. In Fig. 5, taking the CH_4 breakthrough times as an example, the feed flow rates were 300, 500, and 700 ml·min^{-1} at 100 kPa, the CH_4 breakthrough times of the experiment were 330, 200, and 155 s, respectively, and, surprisingly, the simulated CH_4 breakthrough times were close to the experiment data (332, 199, and 152 s) (Fig. 5(a)–(c)). Keeping the feed flow rate fixed at 500 ml·min^{-1}, for adsorption pressures of 100, 200, and 300 kPa (Fig. 5(b), (d), (e)), the simulated CH_4 breakthrough times were 199, 365, and 475 s, respectively, again very similar to the experimental data (200, 360, and 470 s). Moreover, the same phenomenon was observed for N_2 at various adsorption pressures and feed rates, which showed the accuracy of the simulation.

Based on the adjusted adsorption isotherms of CH_4 and N_2 (Fig. 4, solid line), the competitive adsorption isotherms of 75% (vol) CH_4/25% (vol) N_2 were predicted by IAST, which could be considered as the dynamic adsorption isotherms of the mixture. From

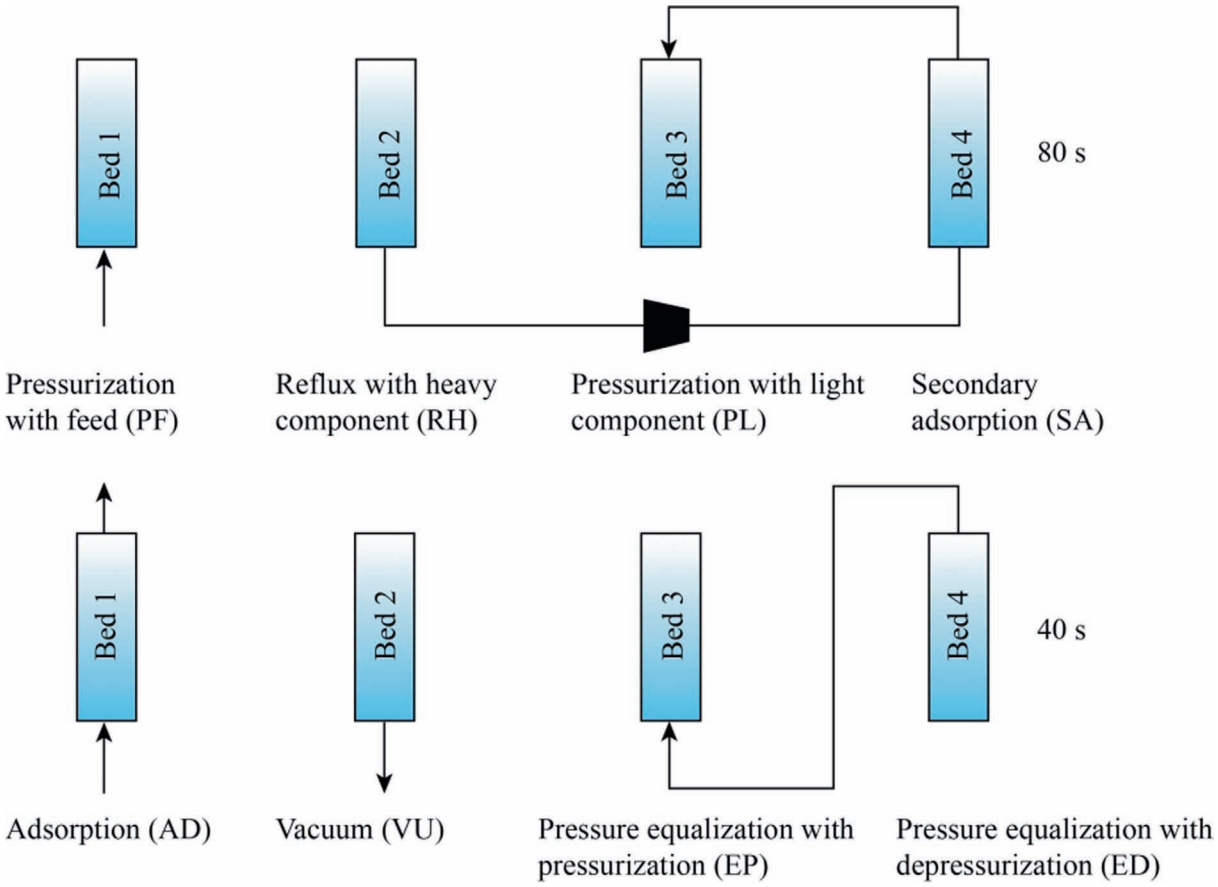

Fig. 8. First 120 s of the operation schedule of the four-bed eight-step PSA.

Table 5
PSA process step timing diagram

Bed	Time/s							
	80	40	80	40	80	40	80	40
Bed 1	PF	AD	SA	ED	RH	VU	PL	EP
Bed 2	RH	VU	PL	EP	PF	AD	SA	ED
Bed 3	PL	EP	PF	AD	SA	ED	RH	VU
Bed 4	SA	ED	RH	VU	PL	EP	PF	AD

Table 6
Comparison of the simulation results of two PSA processes

Ad.*P*/kPa	De.*P*/kPa	Feed rate/L·min^{-1}	Feed gas CH_4%/N_2% (vol)	PSA process	CH_4 purity/%	CH_4 recovery/%
280	10	1.6	75/25	1–3	83	95
				4–8	95	99
			80/20	1–3	88	95
				4–8	99	99

Note: Ad.*P* is adsorption pressure, De.*P* is desorption pressure, 1–3 is single-bed, three-step PSA process, and 4–8 is four-bed, eight-step PSA process.

the breakthrough curves of 75% (vol) CH_4/25% (vol) N_2 at three different pressures of 100, 200, and 300 kPa, the dynamic adsorption capacity of CH_4 in the mixture was also measured. In Fig. 6a, the dynamic adsorption isotherm obtained by simulating breakthrough curves (solid line) was very close to the data directly measured in the breakthrough experiment (dotted line). On the contrary, the adsorption capacity of the mixed gas calculated from the pure component static adsorption isotherm (dashed line) was obviously higher than the dynamic adsorption capacity, which showed the feasibility of this method. As shown in Fig. S2 and Fig. S3 (in Supplementary Material), we applied this method to 55% (vol) CH_4/45% (vol) N_2 mixture and found that it is still suitable. In addition, the gas dynamic adsorption data obtained by this method yielded a line, rather than a single point at a certain pressure.

4.2. Single-bed, three-step PSA experiment and simulation

Based on the static and dynamic adsorption isotherms, a single-bed, three-step PSA was simulated. In Fig. 7, the CH_4 product purity and recovery of PSA in the simulation were compared with the experimental results. When the feed rate was fixed at 2 L·min^{-1}

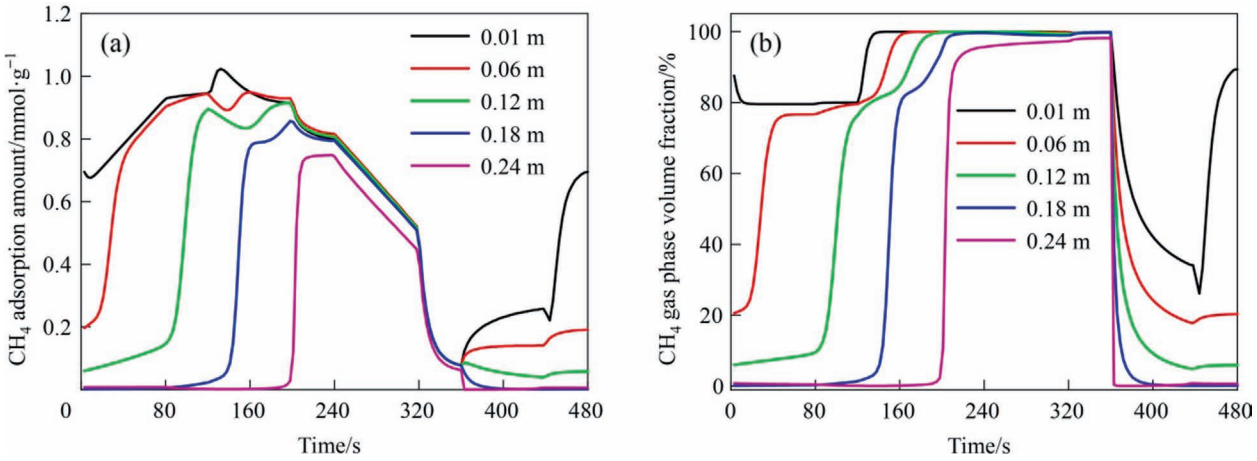

Fig. 9. CH_4 adsorption amount on absorbent (a) and gas phase volume fraction (b) in a single cycle (480 s) of the adsorption bed (75% (vol) CH_4/25% (vol) N_2).

and the adsorption pressure increased from 100 to 200 kPa (Fig. 7 (a)), recoveries were 79% (vol) (115 kPa), 93% (vol) (150 kPa), and 99% (vol) (200 kPa). The simulation results using the dynamic adsorption isotherm (81% (vol), 94% (vol), and 99% (vol)) were very close, whereas simulation results using the static adsorption isotherm showed significant error, amounting to 88% (vol), 97% (vol), and 100% (vol), respectively. In Fig. 7(b), the purities of the CH_4 product showed the same trend: the PSA simulation using dynamic adsorption isotherms was closer to the experiment.

Next, we compared the times required for each step in the PSA simulation and experimental process, especially the time required for PR, as shown in Table 4, and again found the PSA simulation using the dynamic adsorption isotherm to be almost the same as the experiment. For example, the PR time was 100 s (experiment), 100 s (dynamic simulation), and 109 s (static simulation), respectively, at 115 kPa and 1.50 L·min^{-1}. These results confirmed that the dynamic adsorption isotherm obtained by the above method was relatively reliable.

4.3. Four-bed, eight-step PSA simulation

Based on the dynamic adsorption isotherm, a more complicated four-bed, eight-step PSA process was designed to improve the purity and recovery of the CH_4 product. The adsorption bed performed the following eight steps in sequence.

(1) Pressurization with feed (PF).
(2) Adsorption (AD).
(3) Secondary adsorption (SA).
(4) Pressure equalization with depressurization (ED).
(5) Reflux with heavy component (RH).
(6) Vacuum (VU).
(7) Pressurization with light component (PL).
(8) Pressure equalization with pressurization (EP).

A schematic diagram of each step is shown in Fig. 8, and the step sequence of each adsorption bed is shown in Table 5. Taking Bed 1 as an example, the feed gas first entered the bed for pressurization (PF), and the pressure remained constant during the adsorption process (AD). A part of the heavy component gas (CH_4) in Bed 4 was then passed into Bed 1 from the bottom for secondary adsorption (SA). In this way, the bed was further utilized, and the adsorbed N_2 at the bottom of Bed 1 was partially replaced. The top of Bed 1 and the bottom of Bed 2 were then connected for pressure equalization (ED), because the CH_4 content at the top of Bed 1 was relatively high at this time, which prevented CH_4 from being wasted. Through the above steps, the inside of Bed 1 became filled with high purity CH_4. Part of it was refluxed to Bed 3 for adsorption and replacement (RH), and the other part was used as product gas (VU). Finally, Bed 1 was pressurized by the light components flowing out from the top of Bed 2 (PL) and pressure equalization by the pressurization step (EP). For the above complete cycle, the change in bed pressure with time is shown in Fig. S4. With 75% (vol) CH_4/25% (vol) N_2 feed gas (1.6 L·min^{-1}), an adsorption pressure of 280 kPa, and a desorption pressure of 10 kPa, a CH_4 product with 95% (vol) purity and 99% (vol) recovery was obtained. Moreover, under the same conditions, 80% (vol) CH_4/20% (vol) N_2 feed gas was enriched to 99% (vol) purity with 99% (vol) recovery, as shown in Table 6.

In order to analyze CH_4 concentration distribution in the adsorption bed, we simulated CH_4 adsorption amount on the absorbent and the corresponding gas volume fraction at different bed heights. As shown in Fig. 9(a), at the end of the adsorption step at 120 s, the amount of CH_4 adsorbed was very low at the top of the bed, showing inefficient use of the adsorbent. After the second adsorption step from 120 s to 200 s, the bed utilization rate increased significantly. At 240 s, after the pressure equalization with depressurization step, the amount of CH_4 adsorbed at the top of the bed was very close to that at the bottom, indicating that the entire bed was almost fully utilized. Therefore, high purity CH_4 product gas could be obtained after vacuuming. In Fig. 9(b), the CH_4 gas-phase volume fraction was seen to be almost zero at the top of the bed during the adsorption step (80–120 s), indicating that CH_4 would not flow out as waste gas, ensuring its high recovery

5. Conclusions

Applying the static adsorption isotherm of silicalite-1 pellets to simulate the breakthrough and PSA of a 75% (vol) CH_4/25% (vol) N_2 mixture, the results were greatly divergent from the experiment. This was because breakthrough and PSA were both dynamic adsorption processes. The dynamic adsorption isotherm was obtained through mixed gas breakthrough simulations, and through experimental verification of two different concentrations CH_4/N_2 we found that this method was accurate and believed that it could be applied to different concentrations of CH_4/N_2. Based on the dynamic adsorption isotherm, a four-bed, eight-step PSA process was designed, wherein silicalite-1 pellets still performed well in the rejection of N_2 from low quality natural gas. Indeed, the

simulated CH_4 concentration distribution in the adsorption bed indicated why this process produced high purity and excellent recovery of CH_4 from low quality natural gas.

Declaration of Competing Interest

The authors declare that they have no known competing financial interests or personal relationships that could have appeared to influence the work reported in this paper.

Supplementary Material

Supplementary data to this article can be found online at https://doi.org/10.1016/j.cjche.2021.06.028.

Nomenclature

A	specific surface area of the adsorbent, m^{-1}
c_i	gas-phase concentration of component *i*, $mol \cdot m^{-3}$
c_{ps}	specific heat capacity of the adsorbent, $J \cdot mol^{-1} \cdot K^{-1}$
$c_{v,g}$	gas molar constant-volume heat capacity, $J \cdot mol^{-1} \cdot K^{-1}$
D_{ax}	axial dispersion coefficient, $m^2 \cdot s^{-1}$
D_b	bed diameter, m
D_{ki}	Knudsen diffusion coefficient, $m^2 \cdot s^{-1}$
D_m	molecular diffusivity, $m^2 \cdot s^{-1}$
D_{pi}	effective gas-phase pore diffusion coefficient, $m^2 \cdot s^{-1}$
D_V	Molecular diffusion volume, $cm^3 \cdot mol^{-1}$
d	*a*dsorption bed diameter, m
H_0	*a*dsorption bed height, m
ΔH	adsorption heat, $kJ \cdot mol^{-1}$
h_f	heat-transfer coefficient between the gas and solid, $W \cdot m^{-2} \cdot K^{-1}$
h_w	heat-transfer coefficient between the gas and the wall, $W \cdot m^{-2} \cdot K^{-1}$
k_{fi}	film-resistance coefficient, $W \cdot m^{-1} \cdot K^{-1}$
k_i	mass-transfer coefficient, $W \cdot m^{-1} \cdot K^{-1}$
M_i	relative molecular masses of component *i*, $g \cdot mol^{-1}$
Pe	Peclet number
p_i^0	standard-state pressure of pure component *i*, Pa
q_{mi}	equilibrium adsorption amount, $mol \cdot g^{-1}$
q_T	total amount adsorbed, $mol \cdot g^{-1}$
q_i	adsorbed concentration of component *i*, $mol \cdot kg^{-1}$
Re	Reynolds number
r_p	particle radius, m
r_{pore}	average pore size, m
Sc	Schmidt number
Sh	Sherwood number
T_g	gas-phase temperature, K
T_s	solid-phase temperature, K
T_0	ambient temperature, K
v_g	gas velocity, $m \cdot s^{-1}$
μ	dynamic viscosity, $N \cdot s \cdot m^{-2}$
ρ_g	molar gas-phase density, $kg \cdot m^{-3}$
ρ_s	bulk density, $kg \cdot m^{-3}$
ε_b	bed void ratio
ε_p	particle porosity
τ	adsorbent tortuosity factor

References

[1] S. Effendy, C. Xu, S. Farooq, Correction to ‘‘optimization of a pressure swing adsorption process for nitrogen rejection from natural gas”, *Ind. Eng. Chem. Res.* 57 (5) (2018) 1763–1766.

[2] V.I. Águeda Maté, J.A. Delgado Dobladez, S. Álfvvarez-Torrellas, M. Larriba, Á. Martínez Rodríguez, Modeling and simulation of the efficient separation of methane/nitrogen mixtures with $[Ni_3(HCOO)_6]$ MOF by PSA, *Chem. Eng. J.* 361 (2019) 1007–1018.

[3] O. Onel, A.M. Niziolek, J.A. Elia, R.C. Baliban, C.A. Floudas, Biomass and natural gas to liquid transportation fuels and olefins (BGTL+C2_C4): process synthesis and global optimization, *Ind. Eng. Chem. Res.* 54 (1) (2015) 359–385.

[4] S.U. Nandanwar, D.R. Corbin, M.B. Shiflett, A review of porous adsorbents for the separation of nitrogen from natural gas, *Ind. Eng. Chem. Res.* 59 (30) (2020) 13355–13369.

[5] M. Qyyum, K. Qadeer, M. Lee, Comprehensive review of the design optimization of natural gas liquefaction processes: Current status and perspectives, *Ind. Eng. Chem. Res.* 57 (17) (2018) 5819–5844.

[6] R.W. Baker, K. Lokhandwala, Natural gas processing with membranes: An overview, *Ind. Eng. Chem. Res.* 47 (7) (2008) 2109–2121.

[7] M.A. Carreon, Molecular sieve membranes for $N2/CH_4$ separation, *J. Mater. Res.* 33 (1) (2018) 32–43.

[8] Y.D. Cheng, Z.H. Wang, D. Zhao, Mixed matrix membranes for natural gas upgrading: Current status and opportunities, *Ind. Eng. Chem. Res.* 57 (12) (2018) 4139–4169.

[9] Y. Guo, J.L. Hu, X.W. Liu, T.J. Sun, S.S. Zhao, S.D. Wang, Scalable solvent-free preparation of $[Ni_3(HCOO)_6]$ frameworks for highly efficient separation of CH_4 from N_2, *Chem. Eng. J.* 327 (2017) 564–572.

[10] M. Tagliabue, D. Farrusseng, S. Valencia, S. Aguado, U. Ravon, C. Rizzo, A. Corma, C. de Mirodatos, Natural gas treating by selective adsorption: Material science and chemical engineering interplay, *Chem. Eng. J.* 155 (3) (2009) 553–566.

[11] R.T. Yang, Frontmatter. Adsorbents: Fundamentals and Applications, John Wiley & Sons Inc., Hoboken, NJ, USA, 2003.

[12] D.W. Breck, Zeolite Molecular Sieves: Structure, Chemistry, and Use, John Wiley & Sons, New York, 1974.

[13] D. Qu, Y. Yang, Z. Qian, P. Li, J. Yu, A.M. Ribeiro, A.E. Rodrigues, Enrichment of low-grade methane gas from nitrogen mixture by VPSA with CO_2 displacement process: Modeling and experiment, *Chem. Eng. J.* 380 (2020) 122509.

[14] B. Shimekit, H. Mukhtar, Natural gas purification technologies—major advances for CO_2 separation and future directions, In: Adv. Natural Gas Technol. InTech (2012) 235–270.

[15] T. Gao, W. Lin, A. Gu, M. Gu, Coalbed methane liquefaction adopting a nitrogen expansion process with propane pre-cooling, *Appl. Energy* 87 (7) (2010) 2142–2147.

[16] S. Cavenati, C.A. Grande, A.E. Rodrigues, Separation of $CH_4/CO_2/N_2$ mixtures by layered pressure swing adsorption for upgrade of natural gas, *Chem. Eng. Sci.* 61 (12) (2006) 3893–3906.

[17] J.C. Kuo, K.H. Wang, C. Chen, Pros and cons of different Nitrogen Removal Unit (NRU) technology, *J. Nat. Gas Sci. Eng.* 7 (2012) 52–59.

[18] G. Xiao, T.L. Saleman, Y. Zou, G. Li, E.F. May, Nitrogen rejection from methane using dual-reflux pressure swing adsorption with a kinetically-selective adsorbent, *Chem. Eng. J.* 372 (2019) 1038–1046.

[19] T.E. Rufford, S. Smart, G.C.Y. Watson, B.F. Graham, J. Boxall, J.C. Diniz da Costa, E.F. May, The removal of CO_2 and N_2 from natural gas: A review of conventional and emerging process technologies, *J. Petroleum Sci. Eng.* 94–95 (2012) 123–154.

[20] N. Al-Janabi, R. Vakili, P. Kalumpasut, P. Gorgojo, F.R. Siperstein, X.L. Fan, P. McCloskey, Velocity variation effect in fixed bed columns: A case study of CO_2 capture using porous solid adsorbents, *AIChE J.* 64 (6) (2018) 2189–2197.

[21] L. Zhang, Y. Yin, L. Li, F. Wang, Q. Song, N. Zhao, F. Xiao, W. Wei, Numerical simulation of CO_2 adsorption on K-based sorbent, *Energy Fuels* 30 (5) (2016) 4283–4291.

[22] A.-M. Banu, D. Friedrich, S. Brandani, T. Düren, A multiscale study of MOFs as adsorbents in H_2 PSA purification, *Ind. Eng. Chem. Res.* 52 (29) (2013) 9946–9957.

[23] M.S. Shafeeyan, W.M.A.W. Daud, A. Shamiri, N. Aghamohammadi, Modeling of carbon dioxide adsorption onto ammonia-modified activated carbon: Kinetic analysis and breakthrough behavior, *Energy Fuels* 29 (10) (2015) 6565–6577.

[24] Q. Liu, L.Q. Ning, S.D. Zheng, M.N. Tao, Y. Shi, Y. He, Adsorption of carbon dioxide by MIL-101(Cr): Regeneration conditions and influence of flue gas contaminants, *Sci. Rep.* 3 (2013) 2916.

[25] R. Krishna, J.R. Long, Screening metal-organic frameworks by analysis of transient breakthrough of gas mixtures in a fixed bed adsorber, *J. Phys. Chem. C* 115 (26) (2011) 12941–12950.

[26] L.A. Darunte, T. Sen, C. Bhawanani, K.S. Walton, D.S. Sholl, M.J. Realff, C.W. Jones, Moving beyond adsorption capacity in design of adsorbents for CO_2 capture from ultradilute feeds: kinetics of CO_2 adsorption in materials with stepped isotherms, *Ind. Eng. Chem. Res.* 58 (2018) 366–377.

[27] P.G. Aguilera, F.J. Gutiérrez Ortiz, Prediction of fixed-bed breakthrough curves for H_2S adsorption from biogas: Importance of axial dispersion for design, *Chem. Eng. J.* 289 (2016) 93–98.

[28] Q. Al-Naddaf, A.A. Rownaghi, F. Rezaei, Multicomponent adsorptive separation of CO_2, CO, CH_4, N_2, and H_2 over core-shell zeolite-5A@MOF-74 composite adsorbents, *Chem. Eng. J.* 384 (2020) 123251.

[29] L. Erden, A.D. Ebner, J.A. Ritter, Separation of Landfill Gas CH_4 from N_2 Using pressure vacuum swing adsorption cycles with heavy reflux, *Energy Fuels* 32 (3) (2018) 3488–3498.

[30] J.F. Yang, H.H. Bai, H. Shang, J. Wang, J.P. Li, S.G. Deng, Experimental and simulation study on efficient CH_4/N_2 separation by pressure swing adsorption on silicalite-1 pellets, *Chem. Eng. J.* 388 (2020) 124222.

[31] H. Shang, H. Bai, J. Liu, J. Yang, J. Li, PSA simulation and adsorption separation of CH_4-N_2 by self-supporting pellets Silicalite-1, *CIESC J.* 71 (2020) 2088–2098. (in Chinese)

[32] A.L. Myers, J.M. Prausnitz, Thermodynamics of mixed-gas adsorption, *AIChE J.* 11 (1) (1965) 121–127.
[33] K.S. Walton, D.S. Sholl, Predicting multicomponent adsorption: 50 years of the ideal adsorbed solution theory, *AIChE J.* 61 (9) (2015) 2757–2762.
[34] A. Ladshaw, S. Yiacoumi, C. Tsouris, A generalized procedure for the prediction of multicomponent adsorption equilibria, *AIChE J.* 61 (8) (2015) 2600–2610.
[35] S.M. McIntyre, B. Shan, R. Wang, C. Zhong, J. Liu, B. Mu, Monte Carlo simulations to examine the role of pore structure on ambient air separation in metal-organic frameworks, *Ind. Eng. Chem. Res.* 57 (28) (2018) 9240–9253.
[36] C. Goel, H. Bhunia, P.K. Bajpai, Prediction of binary gas adsorption of CO_2/N_2 and thermodynamic studies on nitrogen enriched nanostructured carbon adsorbents, *J. Chem. Eng. Data* 62 (2017) 214–225.
[37] M.D. LeVan, T. Vermeulen, Binary Langmuir and Freundlich isotherms for ideal adsorbed solutions, *J. Phys. Chem.* 85 (22) (1981) 3247–3250.
[38] M. Xu, S. Deng, Efficient screening of novel adsorbents for coalbed methane recovery, *J. Colloid Interface Sci.* 565 (2020) 131–141.
[39] M.S. Santos, C.A. Grande, A.E. Rodrigues, New cycle configuration to enhance performance of kinetic PSA processes, *Chem. Eng. Sci.* 66 (8) (2011) 1590–1599.
[40] T.S. Bhatt, A. Sliepcevich, G. Storti, R. Rota, Experimental and modeling analysis of dual-reflux pressure swing adsorption process, *Ind. Eng. Chem. Res.* 53 (34) (2014) 13448–13458.